Available online at www.sciencedirect.com
ScienceDirect
Journal of Sound and Vibration 299 (2007) 605–620
JOURNAL OF SOUND AND VIBRATION
www.elsevier.com/locate/jsvi

Enhanced iterative learning control for a piezoelectric actuator system using wavelet transform filtering

Chiang-Ju Chien[a,*], Fu-Shin Lee[b], Jhen-Cheng Wang[c]

[a]*Department of Electronic Engineering, Huafan University, Taipei 223, Taiwan*
[b]*Department of Mechatronic Engineering, Huafan University, Taipei 223, Taiwan*
[c]*Research Center, Tungnan Institute of Technology, Taipei 222, Taiwan*

Received 28 September 2005; received in revised form 22 June 2006; accepted 10 July 2006
Available online 29 September 2006

Abstract

For trajectory tracking of a piezoelectric actuator system, an enhanced iterative learning control (ILC) scheme based on wavelet transform filtering (WTF) is proposed in this research. The enhanced ILC scheme incorporates a state compensation in the ILC formula. Combining state compensation with iterative learning, the scheme enhances tracking accuracies substantially, in comparison to the conventional D-type ILC and a proportional control-aided D-type ILC. The wavelet transform is adopted to filter learnable tracking errors without phase shift. Based on both a time–frequency analysis of tracking errors and a convergence bandwidth analysis of ILC, a two-level WTF is chosen for ILC in this study. The enhanced ILC scheme using WTF was applied to track two desired trajectories, one with a single frequency and the other with multiple frequencies, respectively. Experimental results validate the efficacy of the enhanced ILC in terms of the speed of convergence and the level of long-term tracking errors.

1. Introduction

Due to their advantages of infinite small displacement, high stiffness, and wide bandwidth, piezoelectric actuators have been commonly used for precision positioning in various engineering fields, such as positioning of diamond machine tools, positioning of lenses in optics, and positioning of masks in microelectronics. A piezoelectric actuator is made of ferroelectric ceramic materials, typically lead, zirconate and titanate (PZT) compounds. Driven by a dipole electrical field, the crystal structure of the PZT material is polarized and deformed, which results in the excited displacement of the PZT actuator. After removal of the applied electric field, however, a residual polarization or displacement remains within the material. Under repeated driving, the piezoelectric actuator therefore exhibits a nonlinear relation between the input voltage and the output displacement, which is the well-known hysteresis loop.

In recent years, various control schemes have been proposed to compensate for the nonlinear behaviors of piezoelectric systems. Many schemes were based on inversions of certain hysteresis models, e.g. the notable

*Corresponding author. Tel.: +886 2 2663 2102; fax: +886 2 8660 6675.
E-mail address: cjc@huafan.hfu.edu.tw (C.-J. Chien).

0022-460X/$ - see front matter © 2006 Published by Elsevier Ltd.
doi:10.1016/j.jsv.2006.07.021

Preisach model, in the feed-forward path [1], and/or the PID control or the like in the feedback path [2]. More complex control methods such as H-infinity and neural sliding-mode control were also reported [3,4]. All such endeavors have attempted to reduce tracking errors of piezoelectric systems to about 1–5% of stroke lengths.

Some other studies adopted an alternate approach—the iterative learning control (ILC). Basically, the ILC approach utilizes the control input and tracking error information of previous iterations for the purpose of tracking control. No model of the system is required for ILC in general [5]. Compared to other complicated design approaches, the ILC approach takes a reduced effort of control design and implementation. In Ref. [6], the basic P-type ILC was used for the piezoactuator tracking. Its tracking performance for a slow monotonic trajectory was excellent, but the tracking of a sinusoidal trajectory seemed less impressive. In Ref. [7], the basic P-type ILC was applied to track noise disturbed trajectories for a piezoelectric stage under a proportional, integral and derivative (PID) control. It further introduced a disturbance observer to improve tracking accuracies. In Ref. [8], a proportional control-aided ILC scheme was used for position tracking of a piezoelectric motor. It improved tracking errors drastically, compared to a traditional proportional and integral (PI) controller. In Ref. [9], the authors proposed a model-based ILC for tracking control of a piezoelectric actuator. Though it reduced tracking errors significantly in contrast to a phase compensated PI control, the ILC requires a model of the system, which is not desirable in general.

In our experiments of using traditional ILC schemes for trajectory tracking of a piezoelectric actuator system, however, the experimental results were not as expected by the ILC theories. While tracking errors by the traditional D-type ILC scheme were much higher than the floor noise, tracking control by a proportional control-aided ILC scheme even resulted in divergence of the actuator displacement. Therefore, in this study we propose an enhanced ILC scheme based on wavelet transform filtering (WTF). This enhanced ILC scheme differs from traditional ILC significantly. It compensates for the state difference between two consecutive iterations in order that the ILC learning can take place more precisely as desired. Furthermore, it applies the wavelet transform to filter the learnable errors in ILC. The wavelet transform is used as a zero-phase filtering method by decomposing the error signal, de-noising it, and then reconstructing it. Experimental results reveal that tracking errors by the new scheme were quite close to the floor noise.

2. Experimental setup

The experiment platform includes a piezoelectric actuator system, a data acquisition card, and a personal computer. Fig. 1 shows the piezoelectric system for tracking experiments. It includes a piezoelectric actuator stage and a signal conditioning electronics unit. The piezoelectric actuator carries the translation stage and has a displacement range of -8 to 40 μm corresponding to an input voltage of -30 to $+150$ V. The PZT stack of the actuator is pre-stressed in a casing by a compression force of 150 N, and the translation stage is also loaded by a spring. The piezoelectric actuator has a built-in strain gauge sensor with a cable connected to the signal

Fig. 1. The piezoelectric actuator system: a piezoelectric actuator stage with a built-in sensor (in the front), and a driving and sensing electronics unit (in the rear).

conditioning electronics unit. The unit conditions the sensor signal and outputs a sensing voltage of $+0.2$ to -1 V for use by an A/D converter of the data acquisition card. The electronics unit also has a voltage amplifier. The amplifier receives a control input (-1 to $+5$ V) from a D/A converter of the data acquisition card and amplifies it by a gain of 30 to drive the piezoelectric actuator. The A/D and D/A converters of the data acquisition card have 12-bit resolutions. The maximum sampling rate of the A/D converters is 100 K-samples per second, whereas the maximum sampling rate of the D/A converters is 1 K-samples per second. The personal computer executing the control algorithm has a 1-GHz CPU, and the control algorithm is programmed in MATLAB codes under the Windows operating system.

3. Problem statement

The dynamics of the piezoelectric actuator system can be identified as a second-order model coupled with a hysteresis [10]

$$\begin{aligned} m\ddot{p}(t) + b\dot{p}(t) + kp(t) &= k[dv(t) - h(t)], \\ \dot{h}(t) &= \alpha d\dot{v}(t) - \beta|\dot{v}(t)|h(t) - \gamma\dot{v}(t)|h(t)|, \end{aligned} \tag{1}$$

where $v(t)$ and $p(t)$ denote the driving voltage applied to the surfaces of the actuator, and the output displacement of the actuator, respectively; $h(t)$ represents a state variable for modeling the hysteretic dynamics of the actuator; m, b, and k are the effective mass, damping coefficient, and mechanical stiffness of the piezoelectric actuator stage, respectively; d is the effective piezoelectric coefficient related to the slope of the output displacement versus the input voltage of the actuator; and α, β, and γ are parameters that control the shape of the hysteresis loop.

In Ref. [11], system (1) is expressed in the following state-space format for a sinusoidal actuation:

$$\begin{aligned} \dot{x}(t) &= F(x(t)) + Gu(t), \\ y(t) &= Hx(t), \end{aligned} \tag{2}$$

where $u(t)$ and $y(t)$ represent the control input and system output, respectively. In Eq. (2), the state of the system is defined as

$$\begin{aligned} x(t) &= [\,x_1(t) \quad x_2(t) \quad x_3(t) \quad x_4(t) \quad x_5(t)\,]^{\mathrm{T}} \\ &= [\,p(t) \quad \dot{p}(t) \quad h(t) \quad v(t) \quad \dot{v}(t)\,]^{\mathrm{T}}, \end{aligned}$$

and the state-space vectors are given by

$$F(x(t)) = \begin{bmatrix} x_2(t) \\ (-kx_1(t) - bx_2(t) - kx_3(t) + kdx_4(t))/m \\ (\alpha d - \gamma|x_3(t)|)x_5(t) - \beta|x_5(t)|x_3(t) \\ x_5(t) \\ 0 \end{bmatrix},$$

$$G = [0 \quad 0 \quad 0 \quad 0 \quad 1]^{\mathrm{T}},$$

$$H = [1 \quad 0 \quad 0 \quad 0 \quad 0].$$

Obviously, system (2) is nonlinear. If the control task is for the piezoelectric actuator to track a desired trajectory iteratively, system (2) can be discretized and transformed as an iterative discrete-time nonlinear system. It can be then included in the class of iterative discrete-time uncertain nonlinear time-varying systems as follows:

$$\begin{aligned} x_i(n+1) &= f(x_i(n), n) + B(x_i(n), n)u_i(n) + w_i(n), \\ y_i(n) &= C(x_i(n), n)x_i(n) + \xi_i(n), \end{aligned} \tag{3}$$

where i and n denote the indexes in the iteration domain and time domain, respectively; x_i, y_i, and u_i are the system state, system output, and control input, respectively, in iteration i for all $n \in [0, N]$ and for some positive integer N; $C(\cdot,\cdot)$ is time-varying matrix; $f(\cdot,\cdot)$ and $B(\cdot,\cdot)$ are unknown functions; and $w_i(n)$ and $\xi_i(n)$ are input and output disturbances, respectively.

For controlling system (3), a class of iterative learning controllers was proposed in Ref. [12]:

$$u_i(n) = u_i^b(n) + u_i^f(n), \tag{4}$$

where the feedforward controller is

$$u_i^f(n) = \sum_{j=i-m}^{i-m} G_j u_j(n) + \sum_{j=i-1}^{i-m} L_j(n) e_j(n+1), \tag{5}$$

and the feedback controller is given by

$$\begin{aligned} z_i(n+1) &= p(z_i(n)) + q(z_i(n))e_i(n), \\ u_i^b(n) &= r(z_i(n)) + s(z_i(n))e_i(n), \end{aligned} \tag{6}$$

In Eq. (5), $e_j(n+1)$ denotes the tracking error between the desired and system outputs at time $n+1$ in iteration j, and G_j and L_j represent the forgetting factor and learning gain operators, respectively. In Eq. (6), $e_i(n)$ is the current tracking error; and the functions p, q, r, and s are chosen to satisfy some bounded conditions. Two basic controllers of class (4) are, for example, the D-type ILC (abbr. D-ILC):

$$\begin{aligned} u_i(n) &= u_i^f(n), \\ &= u_{i-1}(n) + Le_{i-1}(n+1), \end{aligned} \tag{7}$$

and a proportional control-aided D-type ILC (abbr. PD-ILC):

$$\begin{aligned} u_i(n) &= u_i^f(n) + u_i^b(n) \\ &= u_{i-1}(n) + Le_{i-1}(n+1) + K_p e_i(n), \end{aligned} \tag{8}$$

where L and K_p are the learning gain and proportional gain, respectively. For simplicity, the D-ILC and PD-ILC will be two representative controllers of class (4) in Section 7 for tracking experiments.

In Ref. [12], the convergence analysis of class (4) is based on some restrictive assumptions such as the identical initial condition and the Lipschitz conditions. However, in tracking control of a highly nonlinear system such as the piezoelectric actuator, the assumptions might not be all satisfied and thus the controllers (7) and (8) might not yield tracking results as expected. Therefore, we propose an enhanced ILC (abbr. EILC) that is relieved of the identical initial condition assumption by incorporating state compensation in ILC. The EILC has the update law

$$u_i(n) = u_{i-1}(n) + Le_{i-1}(n+1) + K[e_i(n) - e_{i-1}(n)], \tag{9}$$

where K is the compensation gain. The $K[e_i(n) - e_{i-1}(n)]$ term is designed to offset the state difference between the current and previous iterations at any time n. Since the EILC compensates for the state difference between two consecutive iterations all the time, it does not demand that the initial condition be the same for all iterations. Also, with this state compensation, the iterative learning by the EILC can achieve tracking control of the piezoelectric actuator system more precisely than the D-ILC or PD-ILC, as shown by the experimental results in Section 7. Furthermore, the $Ke_i(n)$ component in Eq. (9) functions as a feedback control that can stabilize the system, similar to the role of $u_i^b(n)$ in Eq. (4).

A note about the causality of ILC is made as follows. In the ILC update laws (5), (7), (8) and (9), the error $e_{i-1}(n+1)$ in iteration $i-1$ is utilized to update the control $u_i(n)$ in iteration i. Since $e_{i-1}(n+1)$ is the tracking error happening before iteration i, the ILC update laws are causal.

4. Wavelet transform filtering for ILC

In the ILC formulae such as Eqs. (7)–(9), a typical learnable term is $e_{i-1}(n+1)$ which is the tracking error caused by the control input $u_{i-1}(n)$ in the previous iteration. This error term is naturally contaminated by

input and output disturbances in a real system, and thus will be filtered before the ILC learns it in the current iteration. To filter the learnable error, the wavelet transform is adopted in this study. The WTF is basically an operation to decompose a noisy signal, de-noise it, and then reconstruct it. To facilitate our approach to the WTF, we will first introduce a two-level WFT structure and derive the transfer function of it, which can be then generalized for any multi-level WTF, as described in the following.

Figs. 2 and 3 show the tree and non-tree structures of the analysis filter bank and the synthesis filter bank, respectively, for two-level wavelet transform [13]. In the two figures, $x(n)$ is the input signal and $\hat{x}(n)$ is the output signal, whereas $d_1(n)$, $d_2(n)$, and $a_2(n)$ are the detail coefficients at level one, the detail coefficients at level two, and the approximation coefficients at level two, respectively. In Fig. 2, H_{a0} and H_{a1} are the lowpass and highpass filters in the analysis bank, respectively, whereas in Fig. 3, H_{s0} and H_{s1} are the lowpass and highpass filters in the synthesis bank, respectively. Also, the up-sampler is denoted by "$\uparrow M$" for an up-sampling of M, and the down-sampler by "$\downarrow M$" for a down-sampling of M, where M is 2 or 4.

The two-level WTF scheme adopted in this study is to decompose $x(n)$, nullify $d_1(n)$ and $d_2(n)$, and then reconstruct the decomposed signal to obtain $\hat{x}(n)$. Therefore, the signal path of the two-level WTF is from the input $x(n)$, through A_2, "$\downarrow 4$", "$\uparrow 4$", and S_2, to the output $\hat{x}(n)$. According to this signal path, we have the

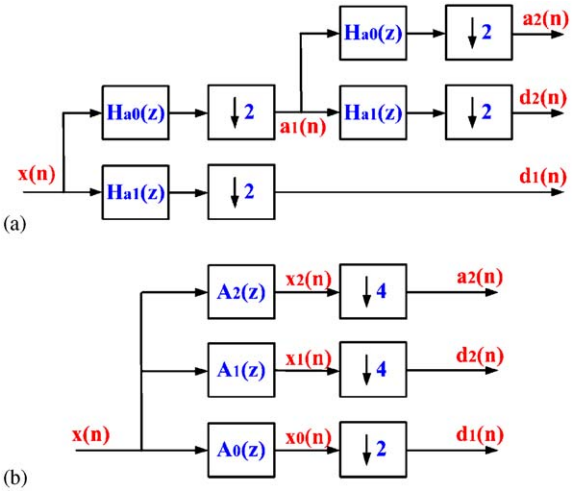

Fig. 2. Analysis filter bank: a two-level analysis filter bank of (a) tree structure and (b) equivalent non-tree structure.

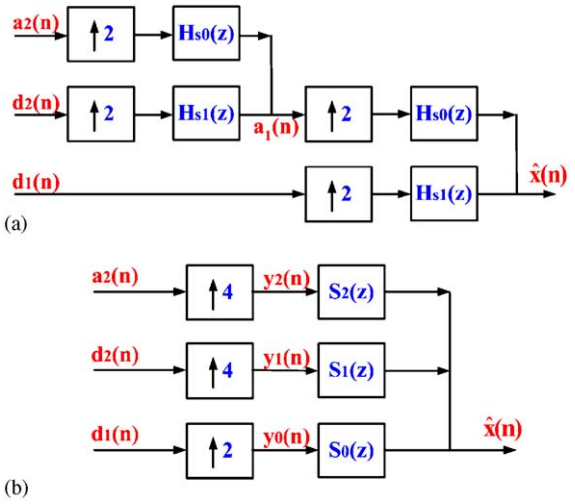

Fig. 3. Synthesis filter bank: a two-level synthesis filter bank of (a) tree structure and (b) equivalent non-tree structure.

z-domain equations

$$X_2(z) = A_2(z)X(z), \tag{10}$$

$$\hat{X}(z) = S_2(z)Y_2(z), \tag{11}$$

where the filters $A_2(z)$ and $S_2(z)$ can be expressed as [13]

$$A_2(z) = H_{a0}(z)H_{a0}(z^2), \tag{12}$$

$$S_2(z) = H_{s0}(z)H_{s0}(z^2). \tag{13}$$

Inserting Eq. (12) into Eq. (10) gives

$$X_2(z) = H_{a0}(z)H_{a0}(z^2)X(z). \tag{14}$$

Inserting Eq. (13) into Eq. (11) yields

$$\hat{X}(z) = H_{s0}(z)H_{s0}(z^2)Y_2(z), \tag{15}$$

Furthermore, it can be shown that the structure of "$\downarrow 4$" cascaded by "$\uparrow 4$" has the following relation between the input and output of the structure [14]:

$$Y_2(z) = \frac{1}{4}\sum_{i=0}^{3} X_2(\mathrm{e}^{-\mathrm{j}2\pi \mathrm{i}/4}z). \tag{16}$$

Inserting Eq. (14) into Eq. (16) produces

$$Y_2(z) = \frac{1}{4}\sum_{i=0}^{3} H_{a0}(\mathrm{e}^{-\mathrm{j}2\pi \mathrm{i}/4}z)H_{a0}((\mathrm{e}^{-\mathrm{j}2\pi \mathrm{i}/4}z)^2)X(\mathrm{e}^{-\mathrm{j}2\pi \mathrm{i}/4}z). \tag{17}$$

Substituting Eq. (17) into Eq. (15) generates

$$\hat{X}(z) = \frac{1}{4}\sum_{i=0}^{3} H_{s0}(z)H_{s0}(z^2)H_{a0}(\mathrm{e}^{-\mathrm{j}2\pi \mathrm{i}/4}z)H_{a0}((\mathrm{e}^{-\mathrm{j}2\pi \mathrm{i}/4}z)^2)X(\mathrm{e}^{-\mathrm{j}2\pi \mathrm{i}/4}z). \tag{18}$$

If the input $X(z)$ is a narrowband signal such that there is no aliasing effect after the down-sampling, it can be fully recovered after the up-sampling and lowpass filtering. This implies the product terms in Eq. (18) are zero for all $i \neq 0$, and thus [14]

$$\hat{X}(z) = \tfrac{1}{4}H_{s0}(z)H_{s0}(z^2)H_{a0}(z)H_{a0}(z^2)X(z). \tag{19}$$

In fact, the sum of the product terms for all $i \neq 0$ in Eq. (18) is named as the alias term in the lowpass branch, according to the perfect reconstruction design using the quadrature mirror filter bank. For perfect reconstruction, this alias term will be cancelled by the other alias term in the highpass branch. On the other hand, the product term for $i = 0$ in Eq. (18), i.e. the product term in Eq. (19), is called the distortion term. For the general case of a wideband input, the influence of the alias term on $\hat{X}(z)$ in Eq. (18) depends on the quality of the lowpass filter $H_{a0}(z^2)$. If $H_{a0}(z^2)$ is an ideal brickwall filter with the cutoff frequency of $\pi/4$ radians/sample, there will be no aliasing around the Nyquist frequency (π radians/sample) after the up-sampling by 4, that is, the alias term will be zero. Now, the purpose of the WTF analysis in this section is to derive the transfer function of the WTF that will be used by the convergence analysis in the next section. In convergence analysis, we can always select a high order filter $H_{a0}(z)$ such that the transition width of $H_{a0}(z^2)$ is narrow enough and thus the aliasing effect after the up-sampling can be neglected. In other words, Eq. (18) can be approximated as Eq. (19) when $H_{a0}(z)$ has a sufficiently high order. Hence we will use Eq. (19) for the following derivation.

Rearranging Eq. (19) leads to the transfer function

$$\frac{\hat{X}(z)}{X(z)} = \frac{1}{4}H_{s0}(z)H_{s0}(z^2)H_{a0}(z)H_{a0}(z^2), \tag{20}$$

for the two-level WTF. However, the wavelet filters (H_{a0}, H_{s0}, H_{a1} and H_{s1}) are typically designed for perfect reconstruction, and the perfectly reconstructed signal by the design has a pure delay:

$$H_{s0}(z)H_{a0}(z) = z^{-d}$$

or

$$H_{s0}(z^2)H_{a0}(z^2) = z^{-2d},$$

where d depends on the type and order of the wavelet family. Since, in ILC it is important that the signal after filtering has zero-phase delay, we can add a phase advance to Eq. (20) and thus obtain the following transfer function of the two-level WTF with no phase lag:

$$\begin{aligned} H(z) &= \frac{\tilde{X}(z)}{X(z)} \\ &= \frac{1}{4} z^{(d+2d)} H_{s0}(z)H_{s0}(z^2)H_{a0}(z)H_{a0}(z^2), \end{aligned} \tag{21}$$

where $\tilde{X}(z)$ denotes the zero-phase WTF output corresponding to an input signal $X(z)$. Finally, we can generalize the above derivation for Eq. (21) and obtain the zero-phase transfer function of any l-level WTF as

$$\begin{aligned} H(z) &= \frac{\tilde{X}(z)}{X(z)} \\ &= \frac{1}{2^l} z^{(2^l-1)d} \left(H_{s0}(z)H_{s0}\left(z^2\right)\ldots H_{s0}\left(z^{2^{l-1}}\right)\right)\left(H_{a0}(z)H_{a0}\left(z^2\right)\ldots H_{a0}\left(z^{2^{l-1}}\right)\right). \end{aligned} \tag{22}$$

In the time domain, the zero-phase WTF relation between an input $x(n)$ and the output $\tilde{x}(n)$ is

$$\tilde{x}(n) = h(n) * x(n), \tag{23}$$

where $h(n)$ is the inverse z-transform of $H(z)$ in Eq. (22), and the notation * means convolution.

In our ILC update laws (7)–(9), the learnable error $e_{i-1}(n+1)$ requires filtering. Thus,

$$\tilde{e}_{i-1}(n+1) = h(n) * e_{i-1}(n+1), \tag{24}$$

according to (23). Based on Eqs. (7)–(9) and (24), we have the ILC implementation equations

$$u_i(n) = u_{i-1}(n) + L\tilde{e}_{i-1}(n+1), \tag{25}$$

$$u_i(n) = u_{i-1}(n) + L\tilde{e}_{i-1}(n+1) + K_p e_i(n), \tag{26}$$

and

$$u_i(n) = u_{i-1}(n) + L\tilde{e}_{i-1}(n+1) + K[e_i(n) - e_{i-1}(n)], \tag{27}$$

for the D-ILC, the PD-ILC, and the EILC, respectively. In Eq. (26), we do not filter the current error $e_i(n)$, since such filtering will cause certain phase delay to the current error, which is not desirable. Similarly in Eq. (27) $e_i(n)$ is not filtered, and thus neither its counterpart $e_{i-1}(n)$.

5. Convergence analysis of ILC

According to Eqs. (25)–(27), we can work on ILC convergence analysis in the frequency domain in order to derive the convergence bandwidth of the D-ILC, PD-ILC, and EILC, respectively. In this paper, let F denote the analog frequency (Hz) and f denote the digital frequency (cycle/sample). We will carry out the convergence analysis of the EILC first, and then of the D-ILC and the PD-ILC.

By inserting Eq. (24) into Eq. (27), one obtains

$$u_i(n) = u_{i-1}(n) + K[e_i(n) - e_{i-1}(n)] + Lh(n) * e_{i-1}(n+1). \tag{28}$$

Taking the z-transform of Eq. (28) leads to

$$U_i(z) = U_{i-1}(z) + K[E_i(z) - E_{i-1}(z)] + LH(z)zE_{i-1}(z). \tag{29}$$

Evaluating Eq. (29) on the unit circle $z = e^{j2\pi f}$ gives rise to

$$U_i(f) = U_{i-1}(f) + K[E_i(f) - E_{i-1}(f)] + LH(f)e^{j2\pi f}E_{i-1}(f). \tag{30}$$

Rearranging Eq. (30) yields

$$U_i(f) = U_{i-1}(f) + G_{ff}(f)E_{i-1}(f) + G_{fb}E_i(f), \tag{31}$$

where

$$G_{fb} = K, \tag{32}$$

$$G_{ff}(f) = -K + Le^{j2\pi f}H(f). \tag{33}$$

By assuming that the plant is linear and has a transfer function $G_p(f)$, the output $Y_i(f)$ in iteration i is

$$Y_i(f) = G_p(f)U_i(f).$$

Hence

$$E_i(f) = Y_d(f) - Y_i(f),$$

or

$$E_i(f) = Y_d(f) - G_p(f)U_i(f), \tag{34}$$

where $E_i(f)$ is the error in iteration i and $Y_d(f)$ is the desired output. Similarly, for iteration $i-1$,

$$E_{i-1}(f) = Y_d(f) - G_p(f)U_{i-1}(f). \tag{35}$$

Then, inserting Eq. (31) into Eq. (34) leads to

$$E_i(f) = \left[Y_d(f) - G_p(f)U_{i-1}(f)\right] - G_p(f) \times \left[G_{ff}(f)E_{i-1}(f) + G_{fb}E_i(f)\right]. \tag{36}$$

Substituting Eq. (35) into Eq. (36) reduces to

$$E_i(f) = E_{i-1}(f) - G_p(f) \times \left[G_{ff}(f)E_{i-1}(f) + G_{fb}E_i(f)\right], \tag{37}$$

Rearranging Eq. (37) produces

$$\frac{E_i(f)}{E_{i-1}(f)} = \frac{1 - G_{ff}(f)G_p(f)}{1 + G_{fb}G_p(f)}. \tag{38}$$

Ideally, learning errors will delay monotonically if

$$\left|\frac{1 - G_{ff}(f)G_p(f)}{1 + G_{fb}G_p(f)}\right| < 1 \quad \forall f. \tag{39}$$

By substituting Eqs. (32) and (33) into Eq. (39), one obtains the convergence criterion:

$$|A(f)| < 1 \quad \forall f, \tag{40}$$

where

$$A(f) = \frac{1 - \left[-K + Le^{j2\pi f}H(f)\right]G_p(f)}{1 + KG_p(f)},$$

i.e.

$$A(f) = 1 - \frac{Le^{j2\pi f}H(f)G_p(f)}{1 + KG_p(f)}, \tag{41}$$

is defined as the convergence argument for the EILC.

In many situations, however, the convergence criterion (40) may not hold for all frequencies. Instead, the inequality may be valid only for frequencies below certain threshold. Hence, we define a convergence bandwidth f_b as the threshold frequency that satisfies

$$|A(f_b)| = 1. \tag{42}$$

If Eq. (42) has multiple real roots, then f_b is the minimal positive root; if Eq. (42) has no real root, f_b is assigned as the Nyquist frequency. It is obvious that, for error convergence, one should pick up a cutoff frequency of filtering that is less than the convergence bandwidth, i.e.

$$f_c < f_b. \tag{43}$$

The convergence analysis of the D-ILC or the PD-ILC is similar, except that the convergence argument is different from (41). It can be shown that the convergence argument is

$$A(f) = 1 - L\mathrm{e}^{\mathrm{j}2\pi f} H(f) G_p(f) \tag{44}$$

for the D-ILC, and

$$A(f) = \frac{1 - L\mathrm{e}^{\mathrm{j}2\pi f} H(f) G_p(f)}{1 + K G_p(f)} \tag{45}$$

for the PD-ILC, respectively.

6. Time–frequency analysis of tracking errors

The ILC convergence analysis imposes the convergence bandwidth as the upper bound of the cutoff frequency for filtering. In implementation of ILC, we can select a cutoff frequency somewhere below the upper bound, such that the signal part of the tracking errors is retrieved whereas the noise part is filtered out. Distinguishing the signal part from the noise part can be accomplished by analysis of the tracking errors. To analyze non-stationary data such as tracking errors, representative methods such as the Short-Time Fourier Transform (STFT), Wavelet Transform (WT), and Wigner–Ville Distribution (WVD) can be applied. In general, the WVD can characterize the time-dependent spectra of the data better than the STFT and WT [15], but it has the drawback of cross-term interference. Nevertheless, the interference problem can be treated by WVD variations, such as the notable smoothed pseudo-WVD [15]. Referring to the ILC study using the time–frequency analysis as in Ref. [16], we adopt the WVD for the analysis of tracking errors. Several basic properties of the WVD are as follows.

The WVD of a signal $x(t)$, denoted as $W_x(t, F)$, is the Fourier transform of the autocorrelation $x(t + (\tau/2))x^*(t - (\tau/2))$:

$$W_x(t, F) = \int_{-\infty}^{\infty} x\left(t + \frac{\tau}{2}\right) x^*\left(t - \frac{\tau}{2}\right) \mathrm{e}^{-\mathrm{j}2\pi F\tau}\, \mathrm{d}\tau, \tag{46}$$

where the superscript * means conjugate. From $W_x(t, F)$, the instantaneous frequency (IF) of $x(t)$, denoted as $F_x(t)$, can be recovered as

$$F_x(t) = \frac{\int_{-\infty}^{\infty} W_x(t, F) F\, \mathrm{d}F}{\int_{-\infty}^{\infty} W_x(t, F)\, \mathrm{d}F}. \tag{47}$$

Due to the frequency marginal property of the WVD, the energy density spectrum (EDS) of $x(t)$, denoted as $|X(F)|^2$, can be obtained using

$$\left|X(F)\right|^2 = \int_{-\infty}^{\infty} W_x(t, F)\, \mathrm{d}t. \tag{48}$$

Furthermore, the smoothed pseudo-WVD (SPWVD) of $x(t)$, denoted as $W'_x(t, F)$, is given by

$$W'_x(t, F) = \int_{\infty}^{\infty} w(\tau) \left[\int_{-\infty}^{\infty} v(t - t') x\left(t' + \frac{\tau}{2}\right) x^*\left(t' - \frac{\tau}{2}\right) \mathrm{d}t' \right] \mathrm{e}^{-\mathrm{j}2\pi F\tau}\, \mathrm{d}\tau, \tag{49}$$

where $w(\cdot)$ and $v(\cdot)$ are smoothing functions such as the Hamming windows.

7. Experiments

Two trajectories for the piezoelectric actuator were tracked using the D-ILC, the PD-ILC, and the proposed EILC, respectively. The first desired trajectory was a single frequency profile with the frequency of 10 Hz and

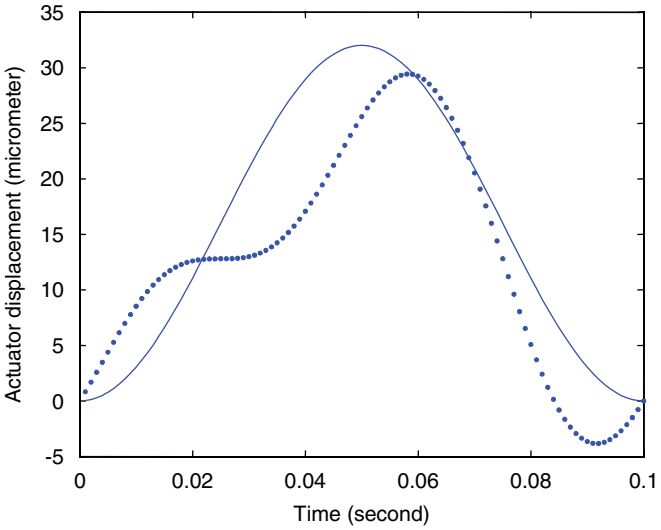

Fig. 4. Desired tracking profiles: a single frequency trajectory (the solid line), and a multi-frequency trajectory (the dotted line).

a stroke length of 32 μm, as shown by the solid line in Fig. 4. The second desired trajectory was a multi-frequency profile with the frequency components of 10 and 20 Hz, and a stroke length of 32 μm, as shown by the dotted line in Fig. 4. Each trajectory was tracked five times per iteration. Besides the initial iteration, there were 100 learning iterations.

In what follows, the digital frequency format is used by default for all the frequency data such as the cutoff frequency, the convergence bandwidth, and the frequency data in the WVD figures. The digital frequency f (cycles/sample) is the analog frequency F (Hz) normalized by the sampling rate (samples/sec). In other words, the analog frequency is equal to the digital frequency times the sampling rate. The nominal sampling rate in the experiments of this study is 500 samples/s. Therefore, $F = 500f$. The Nyquist frequency which is 0.5 cycles/sample as expressed in the digital frequency format is thus 250 Hz in this experimental setup when expressed in the analog frequency format.

7.1. Iterative learning controller design

7.1.1. Learning gain, compensation gain, and proportional gain of ILC

To simply the experiments, we assigned the same value to all the gains: L, K, and K_p. First, the nominal gain g of the piezoelectric actuator system was calculated. It took the value of $-1/5$ by calculating the conversion from the system input of $+5$ V maximum to the system output of -1 V maximum. Then, all the L, K, and K_p gains were given the value of g^{-1}, i.e. -5, for use in the experiments.

7.1.2. Convergence bandwidth of ILC

According to Eqs. (41) and (42), the convergence bandwidth f_b of the EILC can be obtained. Fig. 5a shows the magnitude response of the EILC convergence argument, i.e. $|A(f)|$ versus f, and Fig. 5b shows a corresponding zoom-in plot of the area around $|A(f_b)| = 1$. Fig. 5 was obtained for two-level WTF using Daubechies order-10 (abbr. db10) wavelet filters. In Fig. 5, the solid curve corresponds to a system transfer function of $G_p(f) = g = -1/5$, while the dashed curve corresponds to

$$G_p(f) = \hat{G}_p(f) = \frac{-0.0823e^{-j2\pi f} - 0.0068e^{-j4\pi f} + 0.0564e^{-j6\pi f}}{1 - 0.873e^{-j2\pi f}},$$

where $\hat{G}_p(f)$ was an estimated system transfer function by using a system identification technique. In fact, the EILC convergence bandwidth f_b equals 0.2334 for $G_p(f) = g$, and 0.2354 for $G_p(f) = \hat{G}_p(f)$. The implies that, for two-level WTF using db10 filters, the EILC convergence bandwidth is about 0.23, though the exact transfer function of the system is usually not available. Fig. 6a shows the plot of the EILC convergence

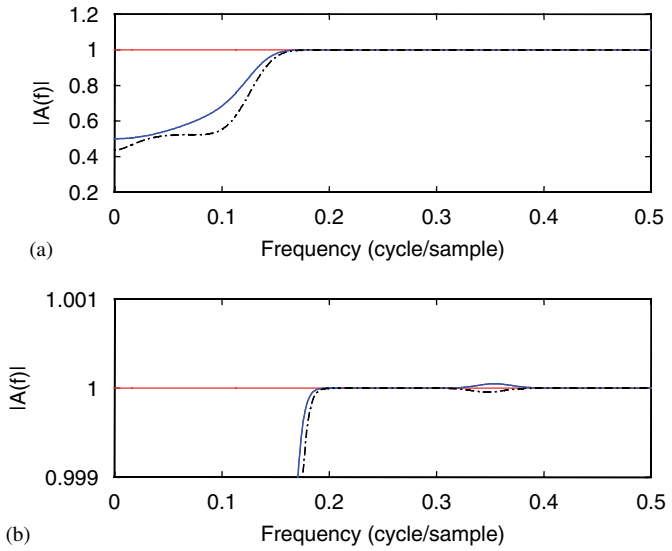

Fig. 5. Convergence argument: magnitude of the EILC convergence argument, $|A(f)|$, vs. frequency, in (a) a full-scale view and (b) a zoom-in view, for $G_p(f)$ equal to g (the solid curve) and $G_p(f)$ equal to $\hat{G}_p$ (the dashed curve), respectively.

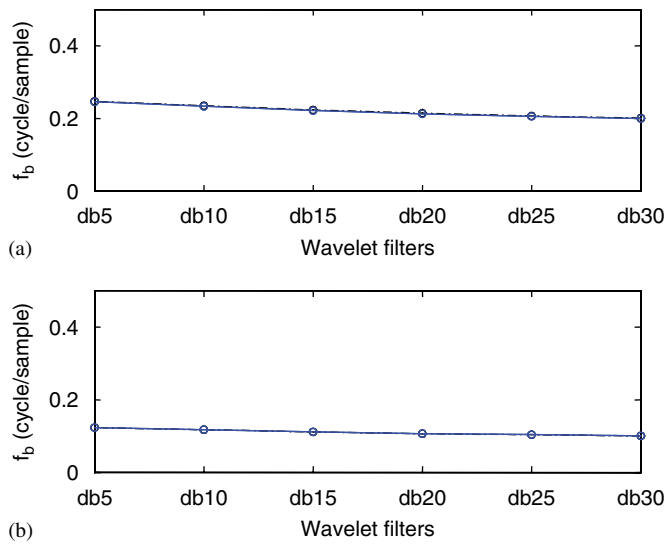

Fig. 6. Convergence bandwidth: EILC convergence bandwidth vs. order of the Daubechies wavelet filters, for (a) two-level WTF and (b) three-level WTF, respectively.

bandwidth versus the order of Daubechies wavelet filters, for two-level WTF. Fig. 6b is the corresponding plot for three-level WTF. One can observe from Fig. 6 that, by using a high-order wavelet family such as the db30, f_b is about 0.2 and 0.1 for two-level and three-level WTF, respectively. In short, the EILC convergence bandwidth is about 0.2 for two-level WTF, and about 0.1 for three-level WTF.

Similarly, by using (44) and (42), one obtains the D-ILC convergence bandwidth that is also about 0.2 and 0.1 for two-level and three-level WTF, respectively. Next, by using (45) and (42), one gets the PD-ILC convergence bandwidth and it is about 0.2 for two-level or three-level WTF.

In summary, the convergence bandwidth of the piezoelectric actuator system is

$$f_b \approx 0.2 \tag{50}$$

for two-level WTF, and

$$f_b \approx 0.1 \text{ min} \tag{51}$$

for three-level WTF, respectively, using either the EILC, D-ILC or PD-ILC.

Finally, we have the following remark on the determination of convergence bandwidth described above. We notice that the convergence bandwidth in this design is not sensitive to different linear estimates of $G_p(f)$. Therefore, we can reasonably suppose that the exact convergence bandwidth of the real piezoelectric actuator is close to what is assumed by (50) and (51). Further, even though the real convergence bandwidth of the system may deviate from (50) and (51) by certain amount, we can tolerate this deviation if the cutoff frequency of the WTF has a substantial margin below the assumed convergence bandwidth (50) and (51).

7.1.3. *Cutoff frequency of WTF*

The cutoff frequency of the WTF is

$$f_c = 1/2^{l+1} \tag{52}$$

for an l-level WTF structure. Hence, by (52) and (50),

$$f_c = 1/8 < f_b \approx 0.2$$

for two-level WTF, which meets the convergence condition (43). Similarly, by (52) and (51),

$$f_c = 1/16 < f_b \approx 0.1 \text{ min}$$

for three-level WTF, which also satisfies (43). It is noted that, in either case, there is a substantial margin between the cutoff frequency and the assumed convergence bandwidth.

In order to choose what level of WTF to use, one can analyze the frequency content of tracking errors. By applying Eqs. (46)–(49) to tracking errors of the piezoelectric system, the frequency characteristics of the errors can be obtained. Fig. 7 shows a set of measured error data, its SPWVD time–frequency content, and the estimations of its EDS and IF, for the piezoelectric system under a PI control as in Ref. [9]. Fig. 8 shows another set of measured error data, its SPWVD time–frequency content, and the estimations of its EDS and

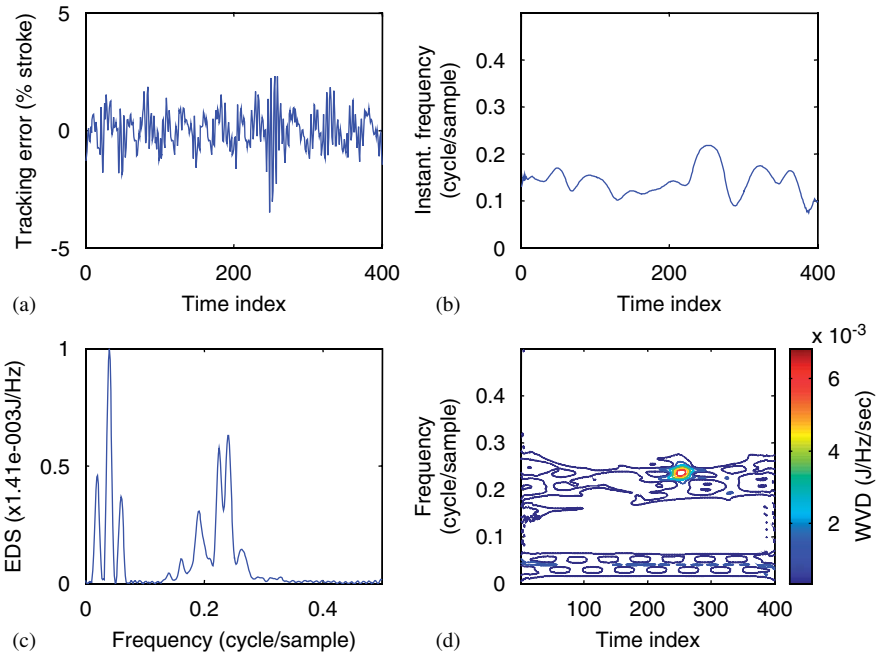

Fig. 7. WVD analysis of tracking errors under a PI control: (a) a record of error measurement; (b) an estimation of the instantaneous frequency; (c) an estimation of the energy density spectrum; (d) the smoothed pseudo-Wigner–Ville Distribution.

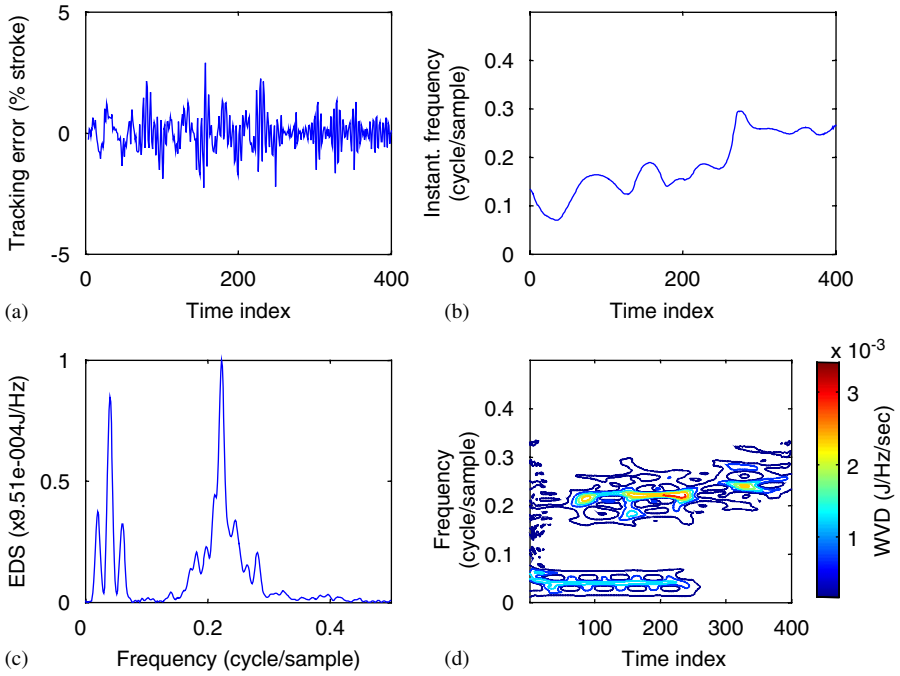

Fig. 8. WVD analysis of tracking errors in a learning iteration: (a) a record of error measurement; (b) an estimation of the instantaneous frequency; (c) an estimation of the energy density spectrum; (d) the smoothed pseudo-Wigner–Ville Distribution.

IF, for the piezoelectric system in a learning iteration as in Ref. [9]. One can observe from Figs. 7 and 8, in particular the SPWVD and EDS plots, that the error data has two major frequency bands: one lower-frequency band below a frequency of about 0.1, and the other higher-frequency band above a frequency of roughly 0.15. It can be reasonably assumed that the lower-band spectra were correlated to the input signal, while the higher-band spectra were caused by the system disturbances.

Therefore, due to the WVD analysis, one should select the two-level WTF. With a cutoff frequency of 1/8, the two-level WTF can retrieve the lower-band signals of tracking errors and filter out the higher-band disturbances.

7.2. Experimental results

Fig. 9 shows typical root-mean-square (rms) tracking errors of the piezoelectric actuator system using the EILC to track the single frequency trajectory for 100 learning iterations. As shown in the figure, the learning transition takes about 3–5 iterations and the steady-state rms tracking errors are about 0.25% of the actuator stroke length. Fig. 10 shows the contrasts of using the D-ILC and the PD-ILC, respectively. It is observed from Fig. 10 that the PD-ILC leads to a divergent actuation, whereas the steady-state rms tracking errors using the D-ILC fluctuate around a mean value of about 0.5% of the stroke length.

Fig. 11 shows an example of tracking errors using the EILC to track the multi-frequency trajectory for 100 learning iterations. Similar to the case of using the EILC to track the single frequency trajectory, tracking errors converge in several iterations and the steady-state rms errors are close to 0.25% of the stroke length. Fig. 12, in contrast, is an example of using the D-ILC and the PD-ILC, respectively, to track the multi-frequency trajectory. As shown in Fig. 12, the output trajectory diverges when the PD-ILC is applied, whereas the steady-state rms errors using the D-ILC vary considerably around a mean of 0.55% stroke.

By comparing Fig. 9 with Figs. 10 and 11 with Fig. 12, it is obvious that the EILC outperforms both the D-ILC and PD-ILC substantially. Furthermore, as shown in Figs. 9 and 11, the steady-state tracking errors by the EILC are close to the system floor noise which is about 0.2% by considering the strain gauge accuracy and the ADC and DAC accuracies. Therefore, the EILC based on WTF is effective in tracking control of the

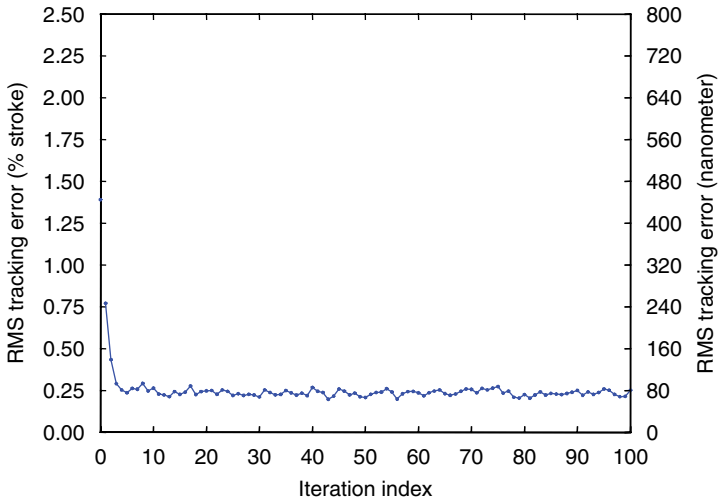

Fig. 9. Tracking errors: rms tracking errors vs. iteration index, for 100 iterations using the EILC to track the single frequency trajectory.

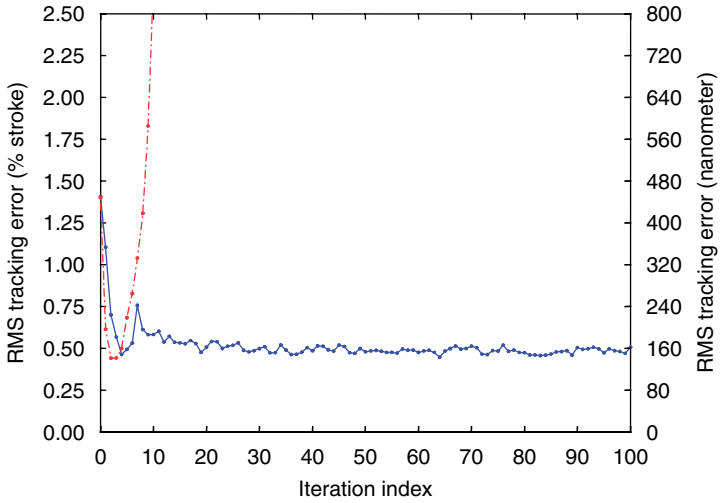

Fig. 10. Tracking errors: rms tracking errors vs. iteration index for 100 learning iterations to track the single frequency trajectory using the D-ILC (the sold line) and the PD-ILC (the dashed line), respectively.

piezoelectric actuator system in terms of the duration of learning transition and the level of steady-state tracking errors. Moreover, the EILC maintained similar performance in experiments even though the L and K gains were varied by ± 2 from the nominal value of -5. This implies that the proposed controller is quite robust.

8. Conclusion

In comparison to the conventional D-ILC and PD-ILC, an EILC scheme is proposed in this study for trajectory tracking of a piezoelectric actuator system. The EILC is an enhancement of traditional ILC by including the state compensation and adopting the WTF for ILC. The state compensation not only relieves the EILC of the constraint that the initial state must be identical for all iterations, but also enhances tracking accuracies compared to the D-ILC and PD-ILC. The wavelet transform is used as a unique method to filter tracking errors without phase lag, so that lower-frequency signals are retrieved for iterative learning while

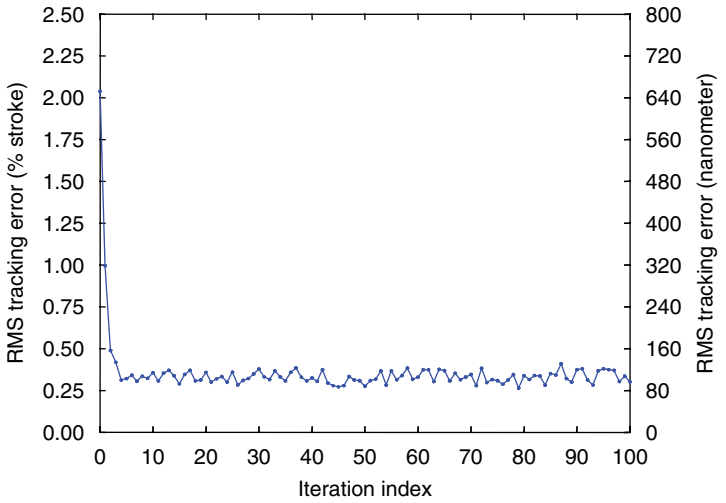

Fig. 11. Tracking errors: rms tracking errors vs. iteration index, for 100 learning iterations using the EILC to track the multi- frequency trajectory.

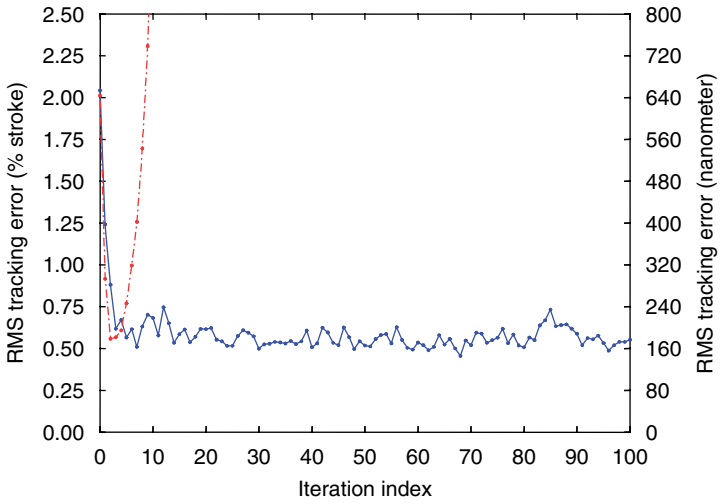

Fig. 12. Tracking errors: rms tracking errors vs. iteration index for 100 learning iterations to track the multi-frequency trajectory using the D-ILC (the sold line) and the PD-ILC (the dashed line), respectively.

higher-frequency noises are attenuated. The differentiation of signals from noises in tracking errors is achieved by using the WVD to analyze the error data. The WVD reveals useful frequency characteristics of the error data, such as the time frequency distribution and the energy density spectrum of the data. Moreover, the convergence analysis of ILC provides the information of the convergence bandwidth. Based on the ILC convergence bandwidth and the time frequency characteristics of the tracking errors, the two-level WTF is selected in this study. The experimental results show that the EILC using WTF not only achieves fast convergence of tracking errors in several iterations but also keeps small steady-state errors that are close to the system noise level.

Acknowledgments

This work was supported by the National Science Council, Taiwan, Republic of China, under Grants NSC93-2218-E-211-002 and NSC93-2212-E-211-007.

References

[1] P. Ge, M. Jouaneh, Tracking control of a piezoceramic actuator, *IEEE Transactions on Control Systems Technology* 4 (1996) 209–216.
[2] J. Tzen, S. Jeng, W. Chieng, Modeling of piezoelectric actuator for compensation and controller design, *Precision Engineering* 27 (2003) 70–86.
[3] S. Salapaka, A. Sebastian, J.P. Cleveland, M.V. Salapaka, Design, identification and control of a fast nanopositioning device, in: *Proceedings of the 2002 American Control Conference*, vol. 3, Anchorage, AK, 2002, pp. 1966–1971.
[4] C.L. Hwang, C. Jan, A reinforcement discrete neuro-adaptive control for unknown piezoelectric actuator systems with dominant hysteresis, *IEEE Transactions on Neural Networks* 14 (1) (2003) 66–78.
[5] Z. Bien, J.X. Xu, *Iterative Learning Control: Analysis, Design Integration and Application*, Kluwer Academic Publishers, Boston, MA, 1998.
[6] K. Leang, S. Devasia, Iterative feedforward compensation of hysteresis in piezo positioners, in: *Proceedings of the 2003 IEEE Conference on Decision and Control,* vol. 3, Maui, Hawaii, 2003, pp. 2626–2631.
[7] Y.C. Huang, C.H. Cheng, Robust tracking control of a novel piezodriven monolithic flexure-hinge stage, in: *Proceedings of the 2004 IEEE Conference on Control Applications*, Taipei, Taiwan, 2004, pp. 977–982.
[8] J.X. Xu, J. Xu, T. Lee, Iterative learning control for a linear piezoelectric motor with a nonlinear unknown input deadzone, in: *Proceedings of the 2004 IEEE Conference on Control Applications*, Taipei, Taiwan, 2004, pp. 1001–1006.
[9] F.S. Lee, C.J. Chien, J.C. Wang, J.J. Liu, Application of a model based iterative learning technique to tracking control of a piezoelectric system, *Asian Journal of Control* 7 (1) (2005) 29–37.
[10] B.M. Chen, T.H. Lee, C. Hang, Y. Guo, S. Weerasooriya, An $H\infty$ almost disturbance decoupling robust controller design for a piezoelectric bimorph actuator with hysteresis, *IEEE Transactions on Control Systems Technology* 7 (2) (1999) 160–174.
[11] C.L. Hwang, Y.M. Chen, C. Jan, Trajectory tracking of large-displacement piezoelectric actuators using a nonlinear observer-based variable structure control, *IEEE Transactions on Control Systems Technology* 13 (1) (2005) 56–66.
[12] C.J. Chien, A discrete iterative learning control for a class of nonlinear time-varying systems, *IEEE Transactions on Automatic Control* 43 (5) (1998) 748–752.
[13] P.P. Vaidyanathan, *Multirate Systems and Filter Banks*, Prentice-Hall, Englewood Cliffs, NJ, 1993.
[14] A. Mertins, *Signal Analysis: Wavelets, Filter Banks, Time–Frequency Transforms and Applications*, Wiley, New York, NY, 1999.
[15] S. Qian, D. Chen, *Joint time–frequency analysis: methods and applications*, PTR Prentice-Hall, Upper Saddle River, NJ, 1996.
[16] Y. Chen and K. Moore, Frequency domain adaptive learning feedforward control, in: *Proceedings of the 2001 IEEE International Symposium on Computational Intelligence in Robotics and Automation*, Banff, Alberta, Canada, 2001, pp. 396–401.